Bull Math Biol (2011) 73:2175–2200
DOI 10.1007/s11538-010-9617-1

ORIGINAL ARTICLE

Modelling Nutrient Uptake by Individual Hyphae of Arbuscular Mycorrhizal Fungi: Temporal and Spatial Scales for an Experimental Design

Andrea Schnepf · Davey Jones · Tiina Roose

Received: 23 April 2010 / Accepted: 9 December 2010 / Published online: 12 January 2011

Abstract Arbuscular mycorrhizas, associations between plant roots and soil fungi, are ubiquitous among land plants. Arbuscular mycorrhizas can be beneficial for plants by overcoming limitations in nutrient supply. Hyphae, which are long and thin fungal filaments extending from the root surface into the soil, increase the volume of soil accessible for plant nutrient uptake. However, no models so far specifically consider individual hyphae. We developed a mathematical model for nutrient uptake by individual fungal hyphae in order to assess suitable temporal and spatial scales for a new experimental design where fungal uptake parameters are measured on the single hyphal scale. The model was developed based on the conservation of nutrients in an artificial cylindrical soil pore (capillary tube) with adsorbing wall, and analysed based on parameter estimation and non-dimensionalisation. An approximate analytical solution was derived using matched asymptotic expansion. Results show that nutrient influx into a hypha from a small capillary tube is characterized by three phases: Firstly, uptake rapidly decreases as the hypha takes up nutrients, secondly, the depletion zone reaches the capillary wall and thus uptake is sustained by desorption of nutrients from the capillary wall, and finally, uptake goes to zero after nutrients held on the capillary wall have been completely depleted. Simulating different parameter regimes resulted in recommending the use of capillaries filled with hydrogel instead of water in order to design an experiment operating over measurable time scales.

A. Schnepf (✉)
Department of Forest and Soil Sciences, BOKU—University of Natural Resources and Life Sciences Vienna, Peter Jordan-Str. 82, 1190 Vienna, Austria
e-mail: andrea.schnepf@boku.ac.at

D. Jones
Environment Centre Wales, Bangor University, Gwynedd LL57 2UW, UK

T. Roose
School of Engineering Sciences, University of Southampton, University Road, Southampton SO17 1BJ, UK

Keywords Experimental design · Fungal nutrient uptake · Mineral weathering · Mycorhizosphere · Phosphorus cycling · Simulation model

1 Introduction

Understanding the mechanistic basis of nutrient cycling in the plant-soil system remains a key goal in predicting ecosystem responses to climate change and the design of sustainable agricultural systems. Quantifying nutrient flow at the soil-root interface, however, represents a major challenge due to the intrinsic biological complexity, high degree of spatial heterogeneity and numerous feedback loops operating in the rhizosphere Jones and Hinsinger (2008). Investigation of nutrient flow in the rhizosphere has proved extremely difficult due to the lack of suitable experimental techniques capable of disentangling multidirectional fluxes at a fine enough scale (Hinsinger et al. 2005). An alternative approach has been the use of mathematical modelling which allows prediction of nutrient flow at the correct spatial and temporal scales as well as allowing the importance of individual factors on plant uptake to be determined (Saleque and Kirk 1995; Tinker and Nye 2000). While this modelling approach has proved successful for agricultural systems associated with high additions of inorganic fertilizer (e.g. KNO_3; Mackay and Barber 1985) and where root uptake is dominated by epidermal cell transport, the models become less robust in low input agroecosystems or in natural systems which rely heavily on organic nutrient inputs. This poor predictive power is due to the lack of inclusion of root strategies which manipulate the rhizosphere to overcome limitations in nutrient supply (e.g. release of organic acids, rhizosphere acidification etc.; Jones et al. 2004). While some of these additional effects have been addressed (Kirk et al. 1999), models including arbuscular mycorrhizas remain in their infancy despite their almost ubiquitous importance in regulating ecosystem function.

Mycorrhizas are symbioses between plant roots and soil fungi where the fungus receives photosynthate from the plant while the plant receives mineral nutrients from the fungus. Other plant benefits are better drought and pathogen resistances; for example. Arbuscular mycorrhizal fungi grow both inside the root cortical cells and in the outside soil where they form very thin filaments around the plant's roots. These filaments are called hyphae and they increase the volume of soil from which nutrients can be absorbed. The relative contributions of roots and fungal hyphae to overall plant nutrient uptake are studied experimentally, e.g., by comparing plant species that form mycorrhizas with nonmycorrhizal mutants that otherwise have the same growth traits, life cycles and responses to nutrient availability (Facelli et al. 2010). However, in spite of the obvious importance of mycorrhizas, mechanistic and spatially explicit models for quantifying the importance of mycorrhizas to plant mineral nutrition remain scarce (Deressa and Schenk 2008; Schnepf and Roose 2006; Schnepf et al. 2008).

Chemical weathering in soil is the dominant natural process delivering new inorganic nutrients to growing plants (McKeague et al. 1986). Moreover, it has been known for decades that mycorrhizas can enhance the dissolution of minerals (Boyle and Voigt 1973). Recently, it was discovered that weatherable minerals (feldspars and

hornblende) present in eluvial (E) horizons of podzols contain abundant narrow tubular pores ranging in diameter from 3–10 μm (Jongmans et al. 1997). These pores are frequently occupied by hyphae, and it has been hypothesized that these hyphae themselves are directly responsible for the mining of the mineral grains. Direct evidence now exists that mycorrhizal hypha are able to penetrate, and most probably create, microsites which are inaccessible to plant roots and which are isolated from bulk soil solution phenomena (Van Breemen et al. 2000). Dissolved products can then be translocated directly to the host plant roots, bypassing the soil solution, and bypassing competition for nutrient uptake by other organisms (Ezawa et al. 2002). In the case of the essential nutrient phosphorus, this view is supported by both experimental investigations (Smith et al. 2003) and mathematical modelling (Schnepf and Roose 2006; Schnepf et al. 2008). Approaches to modelling mineral weathering by fungi are discussed by Rosling et al. (2009).

In order to quantify the contribution of arbuscular mycorrhizal hyphae to nutrient dynamics in soil, information about the extent of the external fungal mycelium as well as the uptake capacity of the individual hyphae is required. A large amount of information is available on rates of nutrient uptake by hyphae of a variety of fungi associated with various host plants (Schweiger and Jakobsen 2000). However, they are based on large scale compartment system experiments and represent an average value for the whole fungal colony. It has been shown experimentally that macroscopic parameters such as the overall hyphal length density are not directly correlated with plant nutrient uptake (Leigh et al. 2009). Schnepf and Roose (2006), Schnepf et al. (2008) have shown in their modelling study that hyphal uptake depends greatly on the uptake parameters of individual hyphae. Therefore, even for the ultimate goal of field scale predictions, single hyphal scale information and careful upscaling (Darrah et al. 2006; Roose and Schnepf 2008) are required in order to make realistic estimations of total phosphorus uptake by mycorrhizal plants. The development of reliable (both experimental and analytical) methods to study physiological uptake properties of hyphae remains a major challenge (Deressa and Schenk 2008).

Our goal in this paper is to complement the Schnepf and Roose (2006) model to enable the accurate prediction and scaling of mycorrhizal derived nutrient uptake in plant-soil systems. In most soils, the diameter of a hypha is smaller than the soil pore diameter. The single hyphal scale model developed in this paper will serve as a basis for a model describing nutrient uptake by a single hypha growing in a soil pore. The model also supports the development of an experimental platform where nutrient uptake by a single hypha growing in a simulated cylindrical soil pore (capillary tube) can be measured. We present a mathematical model for the analysis and interpretation of such data.

2 Materials and Methods

2.1 Developing a Model for Nutrient Uptake by a Single Hypha from a Capillary Tube

We consider a single hypha inside a cylindrical soil pore which is physically equivalent to that of a long capillary tube. We assume that the radius of the capillary tube

is in the same order than that of the hypha, i.e., $r_{\text{tube}}/r_{\text{hypha}} = O(1)$. Furthermore, we can assume that the capillary tube is long compared to its radius as hyphae typically have a radius in the order of 10^{-4} cm (Ezawa et al. 2002) and can be several centimetres long (Tinker and Nye 2000). In this paper we will ignore the fact that in reality the hyphae could be off centre. There are two reasons for this. Firstly, we assume that on average a hypha is at the centre and that variations of it away are not significant. This is realistic since in such small capillaries it is difficult to image that the hyphae would be able to significantly squeeze out the fluid between itself and the capillary wall. Thin water films are notoriously difficult to get rid of under uniform temperature conditions (Ockendon and Ockendon 1995). The second reason is that for the cylindrically symmetric case we are able to derive an analytic solution to the entire problem. Thus, this case is simpler to use when interpreting experimental data. A general geometrical configuration would require more restrictive 3-dimensional computer simulations for each specific geometric configuration. The space between the hypha and the pore wall is filled with either soil solution or an extracellular mucilaginous polysaccharide material similar to that of hydrogel and which is known to be exuded by mycorrhizal hyphae (Abu Ali et al. 1999; Krcmar et al. 1999). Based on existing literature, there are no convincing arguments that water uptake within arbuscular mycorrhizal hyphae is a significant process although the significance of wicking along the hyphal surface remains unclear (Allen 2007). In any case, no figures of water uptake rates per unit surface area of hypha are available. We therefore neglect convective transport and consider radial diffusion towards the hyphal surface where nutrients are taken up according to Michaelis–Menten kinetics (da Silveira and Cardoso 2004; Sharma et al. 1999).

We assume that nutrients are present both in the liquid phase and adsorbed to the pore wall. Hyphae take up nutrients from soil solution. When the hyphal diameter is in the same order as the pore diameter, we need to consider the effect of the pore wall on solute delivery. Due to depletion of solution by the hypha, nutrients are desorbed from the wall of the tube. Assuming that there are no internal nutrient sources or sinks, the equation for radial diffusion of nutrient is given by

$$\frac{\partial C_l}{dt} = D_l \frac{1}{r} \frac{\partial}{\partial r} \left(r \frac{\partial C_l}{\partial r} \right), \tag{1}$$

where C_l is the soil solution concentration in dimensions of mass per unit volume of soil solution and D_l is the effective diffusion coefficient. We assume that the hyphae take up nutrients according to Michaelis–Menten kinetics, so that the boundary condition at the hyphal surface is

$$D \frac{\partial C_l}{dr} = \frac{F_m C_l}{K_m + C_l}, \quad \text{at } r = r_0, \tag{2}$$

where r_0 is the radius of the hypha, F_m is the maximal nutrient influx into the hypha and K_m is the Michaelis–Menten constant.

If the diameter of the tube, r_1, is such that the depletion zone caused by hyphal uptake can reach the tube wall, we assume at this boundary that the flux of nutrient is equal to the rate of change in the density of nutrient bound to the solid surface.

Here, we express the adsorbed concentration C_a per unit surface of pore wall. We derive the boundary condition using conservation of mass. Consider the surface area A of the cylinder with radius $r = r_1$ and unit length. In absence of any source or sink terms, and assuming that we can neglect intra-particle diffusion or surface diffusion, the rate of change of adsorbed concentration must be equal to the flux across the solid-solution interface. Therefore,

$$\frac{d}{dt}\int_A C_a\, dA = -\int_A q \cdot u_n\, dA,$$
$$\text{where } u_n \text{ is the outwards normal vector.} \tag{3}$$

Since C_a is homogeneous on the surface, a unit length of hypha has $\int_A C_a\, dA = 2r_1\pi C_a$. Also, we have $q = -D\frac{\partial C_l}{\partial r}$, $u_n = -1$ and $A = 2r_1\pi$ at $r = r_1$, so that per unit length of hypha, we have $-\int_A q \cdot u_n\, dA = -2r_1\pi D_l \frac{\partial C_l}{\partial r}$. Hence, the boundary condition at $r = r_1$ is

$$\frac{\partial C_a}{\partial t} = -D_l \frac{\partial C_l}{\partial r}. \tag{4}$$

We assume that the rate of change of C_a is given by a first order kinetic reaction:

$$\frac{dC_a}{dt} = k_a C_l - k_d C_a, \tag{5}$$

where k_a and k_d are the ad- and desorption rate constants, respectively.

We now have two equations for the boundary condition at $r = r_1$,

$$D\frac{\partial C_l}{\partial r} = -(k_a C_l - k_d C_a), \tag{6}$$

$$\frac{dC_a}{dt} = k_a C_l - k_d C_a. \tag{7}$$

According to these equations, it is possible that the fungus depletes nutrients from the pore completely, because there is a finite amount of nutrients adsorbed to the surface. In principle, we could add processes that resupply C_l to the pore, such as intra-particle diffusion and dissolution of the mineral wall. However, as a first approximation, we neglect resupply of C_l to the pore. Let us assume that the initial condition for C_l is $C_l = C_{l,0}$ and that, initially, C_{a0} is in equilibrium with C_{l0}, so that $C_{a0} = \frac{k_a}{k_d} C_{l0}$. Here, the quotient $\frac{k_a}{k_d}$ describes a linear relationship between the amount of P adsorbed to the soil phase and its concentration in solution at equilibrium. It is called the buffer power and denoted by $b_P = \frac{k_a}{k_d}$.

In summary, we developed the following model in radial polar coordinates:

$$\frac{\partial C_l}{\partial t} = D_l \frac{1}{r}\frac{\partial}{\partial r}\left(r\frac{\partial C_l}{\partial r}\right), \quad r_0 < r < r_1,\ t > 0, \tag{8}$$

$$D_l \frac{\partial C_l}{\partial r} = \frac{F_m C_l}{K_m + C_l}, \quad r = r_0, \tag{9}$$

$$\begin{cases} D_l \frac{\partial C_l}{\partial r} = -(k_a C_l - k_d C_a), \\ \frac{dC_a}{dt} = k_a C_l - k_d C_a, \quad r = r_1, \end{cases} \tag{10}$$

$$C_l = C_{l0}, \qquad C_a = k_a C_{l0}, \quad t = 0. \tag{11}$$

3 Analysis and Solution of (8)–(11)

3.1 Non-dimensionalisation

For analysis and solution of the model described by (8)–(11), we apply the technique of non-dimensionalisation (Fowler 1997). The same set of dimensionless parameters can be the result of different combinations of dimensional parameters. Therefore, it is more efficient to analyse the dimensionless version of a model.

Let $t = [t]t^*$, $r = [r]r^*$, $C_l = [C_l]C_l^*$ and $C_a = [C_a]C_a^*$. An intrinsic length scale of this system is the hyphal radius, therefore we chose $[r] = r_0$. In addition, let us scale the solution concentration with the Michaelis Menten constant, $[C_l] = K_m$ and the adsorbed concentration with the adsorbed concentration which is in equilibrium with $C_l = K_m$, $[C_a] = \frac{k_a}{k_d} K_m$. Time scales of interest are the time scale of the life of a hypha, which is in the order of several days (Staddon et al. 2003), the reaction time scale that determines how fast the adsorbed nutrient is available for the fungus, and the diffusion time scale. On the diffusion time scale, we scale the time with the factor $[t] = \frac{r_0^2}{D_l}$, and the non-dimensional model in radial polar coordinates is (dropping asterisks)

$$\frac{\partial C_l}{\partial t} = \frac{1}{r} \frac{\partial}{\partial r} \left(r \frac{\partial C_l}{\partial r} \right), \tag{12}$$

$$\frac{\partial C_l}{\partial r} = \lambda \frac{C_l}{1 + C_l}, \quad \text{at } r = 1, \tag{13}$$

$$\begin{cases} \frac{\partial C_l}{\partial r} = -\delta_1 (C_l - C_a), \\ \delta_2 \frac{dC_a}{dt} = C_l - C_a, \quad \text{at } r = r_{\text{end}}, \end{cases} \tag{14}$$

$$C_l = C_a = c_\infty, \quad \text{at } t = 0. \tag{15}$$

The dimensionless parameters are $\lambda = \frac{F_m r_0}{D K_m}$, $\delta_1 = \frac{r_0 k_a}{D_l}$, $c_\infty = \frac{C_{l0}}{K_m}$, $r_{\text{end}} = \frac{r_1}{r_0}$ and $\delta_2 = \frac{D_l}{k_d r_0^2}$, where λ is the dimensionless uptake parameter, c_∞ is the dimensionless nutrient concentration in the bulk solution, r_{end} is the dimensionless distance to the pore wall, and δ_1 and δ_2 are the dimensionless ad- and desorption parameters.

3.2 Parameter Estimation

We parameterise the model with values typical for the case of phosphorus in soil solution. Values for our choice of dimensional model parameters are given in Table 1 and explained in the following paragraphs.

Schweiger and Jakobsen (1999) estimated P uptake parameters that are an order of magnitude larger than root values. We will therefore compare two uptake parameter

Table 1 Typical values of the dimensional parameters for the pore scale model

Parameter	Units	Value for P	Reference
D_l	$\mathrm{cm}^2\,\mathrm{s}^{-1}$	10^{-5}	Lide (2000)
r_0	cm	$2\text{–}5 \times 10^{-4}$	Ezawa et al. (2002)
r_1	cm	$1.2 \times 10^{-1}\text{–}3.5 \times 10^{-3}$	
F_m	$\mu\mathrm{mol}\,\mathrm{cm}^{-2}\,\mathrm{s}^{-1}$	$3.26 \times 10^{-6}\text{–}2.55 \times 10^{-5}$	Tinker and Nye (2000), Schweiger and Jakobsen (1999)
K_m	$\mu\mathrm{mol}\,\mathrm{cm}^{-3}$	$5.8 \times 10^{-3}\text{–}1.7 \times 10^{-3}$	Tinker and Nye (2000), Schweiger and Jakobsen (1999)
b_P	$\mathrm{cm}^3\,\mathrm{cm}^{-3}$	239	Barber (1995)
A	$\mathrm{cm}^2\,\mathrm{cm}^{-3}$	<1000	for sands (Koorevaar et al. 1983)
k_d	s^{-1}	$5.94 \times 10^{-5}\text{–}2.72 \times 10^{-2}$	Chen et al. (1996)
k_a	$\mathrm{cm}\,\mathrm{s}^{-1}$	$1.42 \times 10^{-5}\text{–}6.50 \times 10^{-3}$	$k_a = \frac{k_d b}{A}$ with $A = 1000$
C_{l0}	$\mu\mathrm{mol}\,\mathrm{cm}^{-3}$	$6 \times 10^{-4}\text{–}3 \times 10^{-3}$	low to medium concentration (Barber 1995)

regimes, one with values of roots and one with the larger values as estimated by Schweiger and Jakobsen (1999). For the parameter values given in Table 1, the value of the dimensionless parameter $\delta_2 \gg 1$. The values of r_0 and r_1 in Table 1 suggest that r_{end} can be either $r_{\mathrm{end}} = O(1)$ or $r_{\mathrm{end}} \gg 1$. In the second case, we can treat the domain as semi-infinite, so that the outer boundary has no influence on the flux at the hyphal surface. However, we will only consider the first case when $r_{\mathrm{end}} = O(1)$ in the following simulations. Mycorrhizas tend to increase plant phosphate nutrition when the soil P concentration is low (Tinker and Nye 2000). The values for C_{l0} in Table 1 suggest that in this case we have $c_\infty \ll 1$. We will assume that this is the case in all subsequent calculations. When $c_\infty \ll 1$, the boundary condition at $r = 1$ can be approximated at leading order by the linear equation

$$\frac{\partial C_l}{\partial r} = \lambda C_l, \quad r = 1. \tag{16}$$

Rescaling the concentration $C_l = c_\infty c$ and $C_a = c_\infty c_a$, the model becomes

$$\frac{\partial c}{\partial t} = \frac{1}{r}\frac{\partial}{\partial r}\left(r\frac{\partial c}{\partial r}\right), \tag{17}$$

$$\frac{\partial c}{\partial r} = \lambda c, \quad r = 1, \tag{18}$$

$$\begin{cases} \frac{\partial c}{\partial r} = -\delta_1 (c - c_a), \\ \delta_2 \frac{dc_a}{dt} = c - c_a, \quad \text{at } r = r_{\mathrm{end}}, \end{cases} \tag{19}$$

$$c = c_a = 1, \quad t = 0. \tag{20}$$

3.3 Approximate Analytical Solution

In this section, we develop an approximate analytical solution for the model given by (17)–(20). Because $\delta_2 \gg 1$, we use an asymptotic expansion in $\frac{1}{\delta_2} \ll 1$. This solution is valid for all $t \ll \delta_2$. We call this the inner solution in time; it corresponds to the diffusion time scale. We seek solutions of the form

$$c \approx c_0 + \frac{1}{\delta_2} c_1 + O\left(\frac{1}{\delta_2^2}\right), \tag{21}$$

$$c_a \approx c_{a,0} + \frac{1}{\delta_2} c_{a,1} + O\left(\frac{1}{\delta_2^2}\right). \tag{22}$$

Substituting (21) and (22) into (17)–(20) and collecting the terms of $O(1)$, we get

$$\frac{\partial c_0}{\partial t} = \frac{1}{r}\frac{\partial}{\partial r}\left(r\frac{\partial c_0}{\partial r}\right), \tag{23}$$

$$\frac{\partial c_0}{\partial r} = \lambda c_0, \quad \text{at } r = 1, \tag{24}$$

$$\begin{cases} \frac{\partial c_0}{\partial r} = -\delta_1 (c_0 - c_{a,0}), \\ \frac{dc_{a,0}}{dt} = 0, \quad \text{at } r = r_{\text{end}}, \end{cases} \tag{25}$$

$$c_0 = c_{a,0} = 1, \quad \text{at } t = 0. \tag{26}$$

Because $\frac{dc_a}{dt} = 0$ it follows from the initial condition that $c_a(t) = 1$. Therefore we are left with a model in c_0 only:

$$\frac{\partial c_0}{\partial t} = \frac{1}{r}\frac{\partial}{\partial r}\left(r\frac{\partial c_0}{\partial r}\right), \tag{27}$$

$$\frac{\partial c_0}{\partial r} = \lambda c_0, \quad \text{at } r = 1, \tag{28}$$

$$\frac{\partial c_0}{\partial r} = -\delta_1 (c_0 - 1), \quad \text{at } r = r_{\text{end}}, \tag{29}$$

$$c_0 = 1, \quad \text{at } t = 0. \tag{30}$$

The solution to this model can be found using Laplace transformation. Crank (1975, p. 86) gives the solution to the diffusion equation in a hollow cylinder with general linear boundary conditions and zero initial condition. The approximate analytical solution to (27)–(30) is

$$\begin{aligned} c_0 = 1 + \frac{\lambda[1 - r_{\text{end}}\delta_1 \ln(r/r_{\text{end}})]}{-\lambda - r_{\text{end}}\delta_1 + r_{\text{end}}\lambda\delta_1 \ln(1/r_{\text{end}})} \\ - \pi \sum_{n=1}^{\infty} e^{-\alpha_n^2 t} F(\alpha_n) C_0(r;\alpha_n) \left[\lambda\left\{\delta_1 J_0(r_{\text{end}}\alpha_n) - \alpha_n J_1(r_{\text{end}}\alpha_n)\right\}\right] \end{aligned} \tag{31}$$

where the α_n are the roots of

$$\begin{aligned}&\big[-\lambda J_0(\alpha)-\alpha J_1(\alpha)\big]\big[\delta_1 Y_0(r_{\text{end}}\alpha)-\alpha Y_1(r_{\text{end}}\alpha)\big]\\&\quad-\big[\delta_1 J_0(r_{\text{end}}\alpha)-\alpha J_1(r_{\text{end}}\alpha)\big]\big[\lambda Y_0(\alpha)-\alpha Y_1(\alpha)\big]=0,\end{aligned}\tag{32}$$

$$\begin{aligned}F(\alpha_n)=&\big(\delta_1 J_0(r_{\text{end}}\alpha_n)-\alpha_n J_1(r_{\text{end}}\alpha_n)\big)\\&\times\Big\{\big[\delta_1 J_0(r_{\text{end}}\alpha_n)-\alpha_n J_1(r_{\text{end}}\alpha_n)\big]^2\big(\lambda^2+\alpha_n^2\big)\\&-\big[-\lambda J_0(\alpha_n)-\alpha_n J_1\alpha_n\big]^2\big(\delta_1^2+\alpha_n^2\big)\Big\}^{-1},\end{aligned}\tag{33}$$

and

$$\begin{aligned}C_0(r,\alpha_n)=&J_0(r\alpha_n)\big[-\lambda Y_0(\alpha_n)-\alpha_n Y_1(\alpha_n)\big]\\&-Y_0(r\alpha_n)\big[-\lambda J_0(\alpha_n)-\alpha_n J_1(\alpha_n)\big].\end{aligned}\tag{34}$$

In the limit $t\to\infty$, the solution is

$$c_{\text{lim}}=\frac{r_{\text{end}}\delta_1+r_{\text{end}}\delta_1\lambda\ln(r)}{\lambda+r_{\text{end}}\delta_1+r_{\text{end}}\delta_1\lambda\ln(r_{\text{end}})}.\tag{35}$$

In Fig. 1, (31) is plotted against the numerical solution of the full non-linear problem. The numerical scheme was obtained using a finite difference scheme with a centered discretisation in space and the θ-method in time. Due to the non-linear boundary condition, we have an implicit non-linear expression, which we solved by fixed-point iteration. The numerical and analytical solutions agree well, so we are confident in our use of the approximate analytical solution. At $t=100$, the solution has reached the limit where the analytic solution given by (31)–(34) becomes invalid. This is consistent with the condition for the validity of this approximate solution that $t\ll\delta_2$, where $\delta_2=4000$.

To get the solution for times $t\gg\delta_2$, we rescale time and let $t=\delta_2\tau$, so that the model becomes

$$\frac{1}{\delta_2}\frac{\partial c}{\partial\tau}=\frac{1}{r}\frac{\partial}{\partial r}\left(r\frac{\partial c}{\partial r}\right),\tag{36}$$

$$\frac{\partial c}{\partial r}=\lambda c,\quad\text{at } r=1,\tag{37}$$

$$\begin{cases}\frac{\partial c}{\partial r}=-\delta_1(c-c_a),\\ \frac{dc_a}{d\tau}=c-c_a,\quad\text{at } r=r_{\text{end}},\end{cases}\tag{38}$$

$$c\approx c_{\text{lim}},\qquad c_a,\approx 1,\quad\text{at } \tau\approx 0.\tag{39}$$

The initial conditions (39) come from matching with the solution of the diffusion time scale model as $t\to\infty$. There we saw that, at leading order, $c_{a,0}=1$ for all times, and $c_0=c_{\text{lim}}$ as $t\to\infty$.

Using asymptotic expansions in $\frac{1}{\delta_2}\ll 1$, we obtain an approximate solution which we call the outer solution in time and which corresponds to the binding reaction time

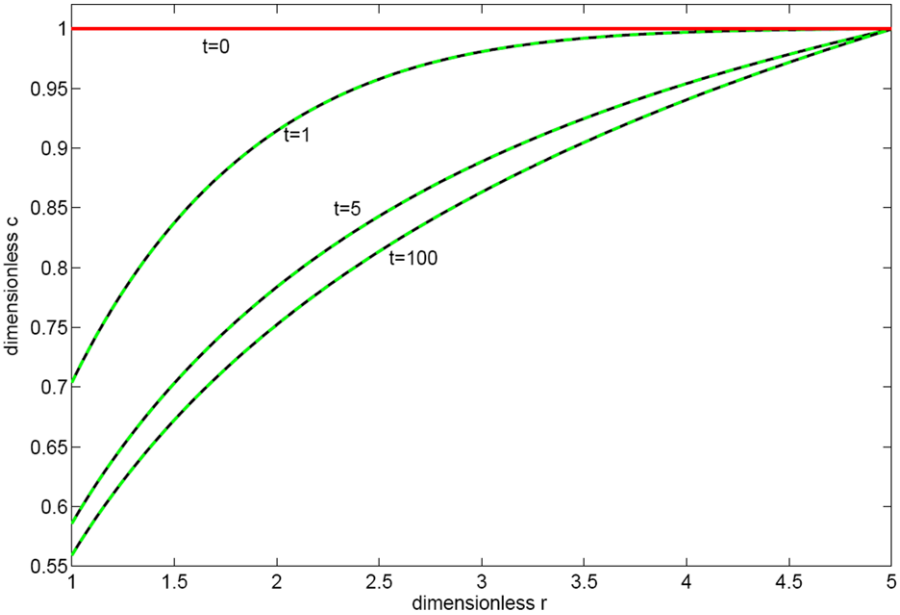

Fig. 1 Plot of (31) (*solid line*) against numerical solution of full non-linear model (12)–(15) (*dashed line*). Model parameters: $\lambda = 0.5$, $\delta_1 = 0.6$, $\delta_2 = 4000$, $r_0 = 1$, $r_1 = 5$. Numerical parameters: $\Delta x = 0.04$, $\Delta t = 0.0016$

scale. We seek solutions of the form

$$c \approx c_0 + \frac{1}{\delta_2} c_1 + O\left(\frac{1}{\delta_2^2}\right), \tag{40}$$

$$c_a \approx c_{a,0} + \frac{1}{\delta_2} c_{a,1} + O\left(\frac{1}{\delta_2^2}\right). \tag{41}$$

Substituting (40) and (41) into (36)–(39) and collecting the terms of $O(1)$, we get

$$0 = \frac{1}{r}\frac{\partial}{\partial r}\left(r\frac{\partial c_0}{\partial r}\right), \tag{42}$$

$$\frac{\partial c_0}{\partial r} = \lambda c_0, \quad \text{at } r = 1, \tag{43}$$

$$\begin{cases} \frac{\partial c_0}{\partial r} = -\delta_1 (c_0 - c_{a,0}), \\ \frac{dc_{a,0}}{d\tau} = c_0 - c_{a,0}, \quad \text{at } r = r_{\text{end}}, \end{cases} \tag{44}$$

$$c_{a,0} = 1, \quad \tau \approx 0. \tag{45}$$

The solution of (42) is

$$c_0(r, \tau) = B_1 \ln(r) + B_2, \tag{46}$$

where B_1 and B_2 are constants of integration to be determined from the two boundary conditions. From the boundary condition at $r = 1$ we get that

$$\left.\frac{dc_0}{dr}\right|_{r=1} = B_1(\tau) = \lambda c_0(1, \tau). \tag{47}$$

Because $\ln(1) = 0$, we get also that at $r = 1$, (46) becomes $c_0(1, \tau) = B_2$. Hence $B_1 = \lambda B_2(\tau)$ so that we can express the solution as

$$c_0(r, \tau) = B_2 \lambda \ln(r) + B_2. \tag{48}$$

From the boundary condition at $r = r_{\text{end}}$, we get

$$\left.\frac{dc_0}{dr}\right|_{r=r_{\text{end}}} = \frac{\lambda B_2}{r_{\text{end}}} = -\delta_1 \left(\lambda B_2 \ln(r_{\text{end}}) + B_2 - c_{a,0}\right). \tag{49}$$

Hence, we obtain an expression for B_2 with respect to $c_{a,0}$:

$$B_2 = \frac{\delta_1 r_{\text{end}}}{\lambda + \delta_1 r_{\text{end}} \lambda \ln(r_{\text{end}}) + \delta_1 r_{\text{end}}} c_{a,0}. \tag{50}$$

Substituting (50) into (48) and substituting the result into the equation for $c_{a,0}$ in (44), we get the following linear ordinary differential equation

$$\frac{dc_{a,0}}{d\tau} + \gamma c_{a,0} = 0, \tag{51}$$

with initial condition $c_{a,0}(0) = 1$, where

$$\gamma = 1 - \frac{(\lambda \ln(r_{\text{end}}) + 1)\delta_1 r_{\text{end}}}{\lambda + \delta_1 r_{\text{end}} \lambda \ln(r_{\text{end}}) + \delta_1 r_{\text{end}}}. \tag{52}$$

The solution is

$$c_{a,0} = e^{-\gamma \tau}. \tag{53}$$

Substituting this into (51), B_2 is

$$B_2 = \frac{\delta_1 r_{\text{end}}}{\lambda + \delta_1 r_{\text{end}} \lambda \ln(r_{\text{end}}) + \delta_1 r_{\text{end}}} e^{-\gamma \tau}, \tag{54}$$

and the solution for c_0 becomes

$$c_0 = \frac{\delta_1 r_{\text{end}} [\lambda \ln(r) + 1]}{\lambda + \delta_1 r_{\text{end}} \lambda \ln(r_{\text{end}}) + \delta_1 r_{\text{end}}} e^{-\gamma \tau}. \tag{55}$$

This approximate analytical solution was compared to the numerical solution of the full non-linear model (12)–(15) but with the time expressed in terms of τ. The result is shown in Fig. 2; the analytical solution agrees well with the numerical solution. Therefore, we are confident in our use of this approximate analytical solution in the following simulations.

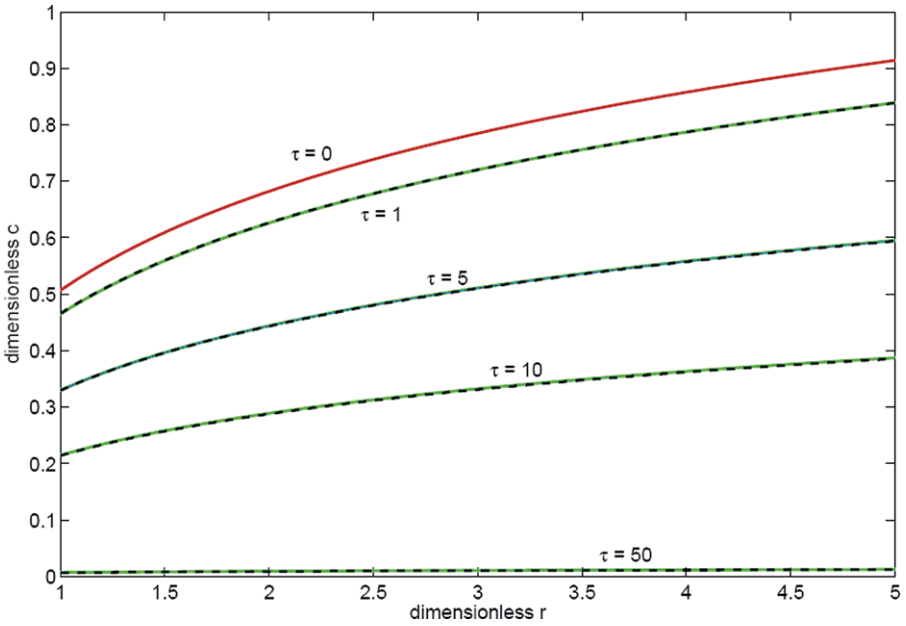

Fig. 2 Plot of (56) (*solid line*) against numerical solution of full model (12)–(15) (*dashed line*). Model parameter: $\lambda = 0.5$, $\delta_1 = 0.6$, $\delta_2 = 4000$, $r_0 = 1$, $r_1 = 5$. Numerical parameter: $\Delta x = 0.04$, $\Delta\tau = 0.0016$

For the example given in Fig. 3, the equilibrium concentration $c_0 = 0$ is reached fast. In dimensional terms (based on the parameter values on Table 1), it is reached after approximately 1.5 hrs, which means that within this time, the fungus has completely exhausted all the available nutrients in the pore. This is related to the fast reaction time. The fungus would require a longer time to take up all available nutrients if the desorption reaction was slower.

The composite solution valid at all times is obtained as the sum of the outer and the inner solution minus the common part, i.e. the concentration at $r = 1$ is

$$c = 1 + \frac{\delta_1 r_{\text{end}}[e^{-\gamma\tau} - 1 - \lambda \ln(r_{\text{end}})] - \lambda}{\lambda + r_{\text{end}}\delta_1 + r_{\text{end}}\lambda\delta_1 \ln(r_{\text{end}})} - \pi \sum_{n=1}^{\infty} e^{-\alpha_n^2 \delta_2 \tau} F(\alpha_n) C_0(1; \alpha_n) \left[\lambda\left\{\delta_1 J_0(r_{\text{end}}\alpha_n) - \alpha_n J_1(r_{\text{end}}\alpha_n)\right\}\right], \quad (56)$$

where the α_n are the positive roots of (32) and $F(\alpha_n)$ and C_0 are given by (33) and (34) when $r = 1$.

Based on this, the dimensionless influx into the hypha is given by

$$F(\tau) = \lambda c_\infty c = \lambda c_\infty \left[1 + \frac{\delta_1 r_{\text{end}}[e^{-\gamma\tau} - 1 - \lambda \ln(r_{\text{end}})] - \lambda}{\lambda + r_{\text{end}}\delta_1 + r_{\text{end}}\lambda\delta_1 \ln(r_{\text{end}})}\right.$$

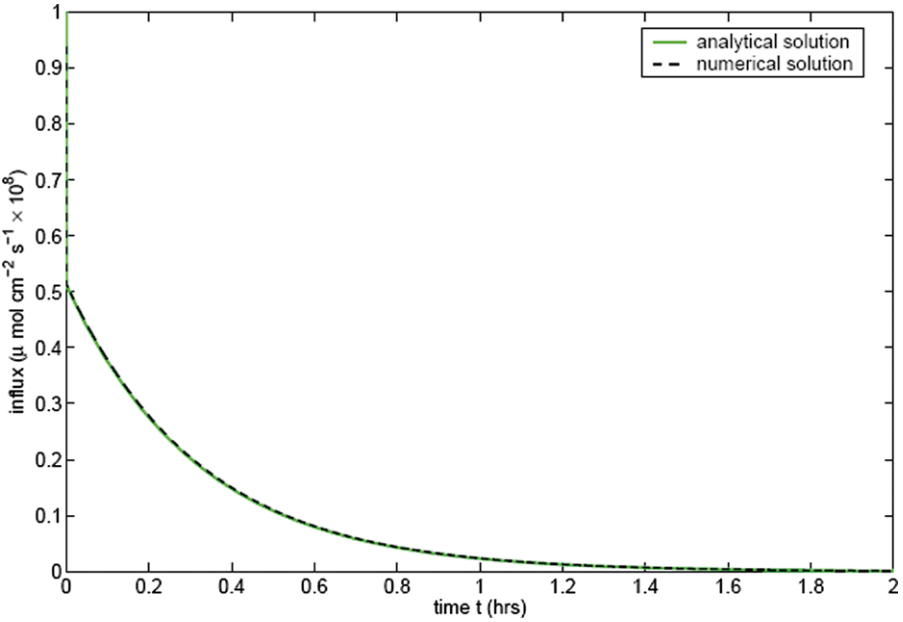

Fig. 3 Approximate analytical and numerical solution for nutrient influx into hypha. Model parameters: $\lambda = 0.5$, $\delta_1 = 0.6$, $\delta_2 = 4000$, $r_0 = 1$, $r_1 = 5$. Numerical parameters: $\Delta x = 0.04$, $\Delta\tau = 0.0016$ and $\Delta\tau = 1 \times 10^{-6}$ during the first five seconds

$$
\begin{aligned}
&- \pi \sum_{n=1}^{\infty} e^{-\alpha_n^2 \delta_2 \tau} F(\alpha_n) C_0(1; \alpha_n) \\
&\times \left[\lambda \left\{ \delta_1 J_0(r_{\text{end}} \alpha_n) - \alpha_n J_1(r_{\text{end}} \alpha_n) \right\} \right] \Bigg]. \qquad (57)
\end{aligned}
$$

The scaling for the flux is $\frac{DK_m}{r_0} = \frac{F_m}{\lambda}$ and the scaling for time in terms of τ is $\frac{1}{k_d}$. Therefore, the dimensional influx into the hypha is $F_D(t_D) = \frac{F_m}{\lambda} F(k_d t_D)$.

$$
\begin{aligned}
F_D(t_D) = F_m c_\infty \Bigg[1 &+ \frac{\delta_1 r_{\text{end}} [e^{-\gamma k_d t_D} - 1 - \lambda \ln(r_{\text{end}})] - \lambda}{\lambda + r_{\text{end}} \delta_1 + r_{\text{end}} \lambda \delta_1 \ln(r_{\text{end}})} \\
&- \pi \sum_{n=1}^{\infty} e^{-\alpha_n^2 \delta_2 k_d t_D} F(\alpha_n) C_0(1; \alpha_n) \\
&\times \left[\lambda \left\{ \delta_1 J_0(r_{\text{end}} \alpha_n) - \alpha_n J_1(r_{\text{end}} \alpha_n) \right\} \right] \Bigg], \qquad (58)
\end{aligned}
$$

where $\lambda = \frac{F_m r_0}{D_l K_m}$, $\delta_1 = \frac{r_0 k_a}{D_l}$, $c_\infty = \frac{C_{l0}}{K_m}$, $r_{\text{end}} = \frac{r_1}{r_0}$, $\delta_2 = \frac{D_l}{k_d r_0^2}$ and t_D is the dimensional time.

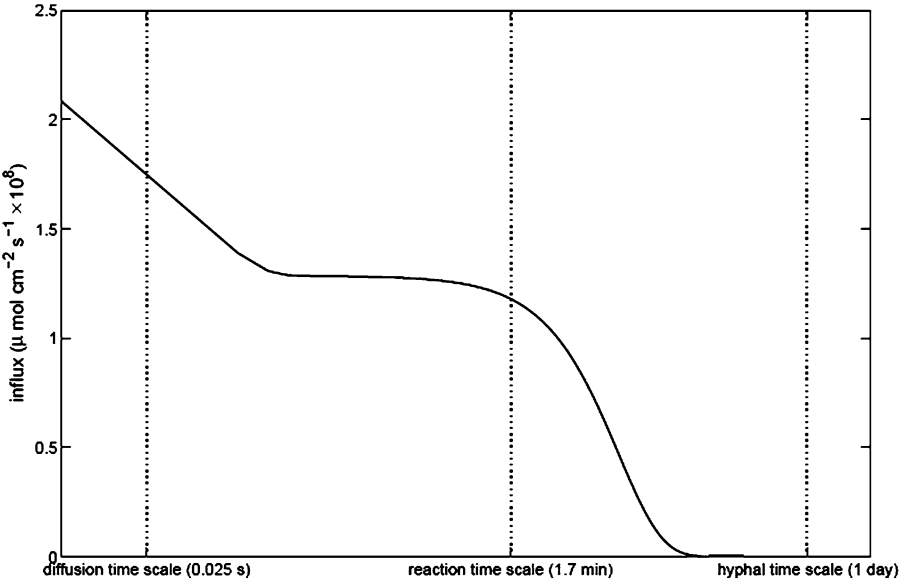

Fig. 4 Phases of phosphate influx into a single hypha as calculated by the bounded pore model

4 Results and Discussion

Rates of arbuscular mycorrhizal hyphal growth in soil are known to be relatively rapid and similar in magnitude to those of roots (0.5–3 mm d^{-1}; Jakobsen et al. 1992). Whilst these rates of hyphal expansion suggest rapid exploitation of the soil volume, our knowledge of nutrient depletion rates by hyphae has been limited to large scale measurements (on the mm to cm scale). This scale of measurement, however, is far removed from the spatial scale at which hyphae largely operate (µm to mm scale). Experimentally measuring hyphal-mediated nutrient depletion from micropores in a complex soil matrix, however, is currently not possible. Consequently, we have little idea of the times taken for hyphae to exploit soil pores of different volumes and wall chemistries. Here we present a model for a relatively immobile nutrient which suggests that hyphae can rapidly deplete P from soil micropores. This result is consistent with the rapid rates of hyphal growth and turnover reported in Staddon et al. (2003).

Figure 4 points out the phases of phosphate uptake by a single hypha from a capillary tube, approximating a uniform cylindrical soil pore, using parameter values from Table 1. Time is plotted on a logarithmic scale for better visualisation. The speed at which P uptake takes place depends on the values of the ad- and desorption as well as uptake parameters. At a time scale in the order of the solute diffusion time scale $t_{\text{diffusion}} = r_0^2/D_l$ (in this example 0.025 s), the flux rapidly decreases as the hypha takes up P, creating a depletion zone around it. At a time scale in the order of the reaction time scale, $t_{\text{reaction}} = 1/k_d$ (in this example 1.7 min), the depletion zone has reached the outer boundary at the pore wall and the concentration in the pore water solution is sustained with nutrients that are desorbed from the pore wall. After the adsorbed phase has also been depleted by the fungus, the concentration in the solution

tends to zero, which is the equilibrium concentration reached at a time much larger than the reaction time scale.

The model described here can provide information for the design of single hyphal scale experiments by estimating a range of parameter values for an optimal experimental setup. Such an experimental setup would be useful for validating single hyphal scale nutrient acquisition models which would ultimately have broad application (e.g. for optimization of nutrient supply rates, inclusion in mineral weathering models, prediction of carbon flow in plant-soil systems). In the model described here we portray a hypha entering a long cylindrical pore which experimentally could be matched by glass capillaries. We focus on the study of P uptake from this capillary by a hypha. We sought to represent an experimental system such that its dynamics occurs on practicable time scales and that concentrations and fluxes are within detection limits of current analytical methods. Properties of the capillary wall, and thus the reaction time scale, could be manipulated by applying different coatings to the capillary walls (e.g. different (oxy)hydroxides of Al and Fe). Diffusion time scale could be manipulated by using different hydrogels instead of water solutions which would have a different diffusion coefficient or by using hyphae of different radii, although this is of course harder to control. Varying the spatial dimensions (capillary radius) or the initial P concentration in solution/hydrogel changes the time at which final zero equilibrium is reached and the magnitude of the uptake rate, respectively. All these effects are illustrated in Figs. 5–10. One by one, the effects of varying the model parameters are shown, starting with a default parameter set of $k_d = 3 \times 10^{-2}\ \mathrm{s}^{-1}$, $C_0 = 1 \times 10^{-4}\ \mu\mathrm{mol\,cm}^{-3}$, $D_l = 1 \times 10^{-5}\ \mathrm{cm}^2\,\mathrm{s}^{-1}$, $b_p = 239$, $r_0 = 5 \times 10^{-4}$ cm, $r_1 = 25 \times 10^{-4}$ cm. Hence, default diffusion and reaction time scales in this example are 0.025 s and 0.56 min, respectively. In addition, two different capacities of the fungus to take up P are considered: (a) Fungal uptake parameter values similar to those of a plant (Tinker and Nye 2000): $K_m = 5.8 \times 10^{-3}\ \mu\mathrm{mol\,cm}^{-3}$, $F_m = 3.26 \times 10^{-6}\ \mu\mathrm{mol\,cm}^{-2}\,\mathrm{s}^{-1}$, and (b) larger fungal uptake parameter values as estimated by Schweiger and Jakobsen (1999): $K_m = 1.7 \times 10^{-3}\ \mu\mathrm{mol\,cm}^{-3}$, $F_m = 2.55 \times 10^{-5}\ \mu\mathrm{mol\,cm}^{-2}$. They do not affect the diffusion or reaction time scale; however, they do affect the magnitude of P influx which could be of importance with respect to the measurement method, i.e., detection limit.

The effect of varying the value of the desorption rate constant k_d is shown in Fig. 5. This parameter is related to the speed of P desorption from the capillary wall. It shows that when desorption is slow, the concentration in the soil solution is sustained at a lower value, but over a longer period of time. Decreasing the value of k_d by one and two orders of magnitude increases the reaction time scale from the default value of 0.56 min to 5.56 min and 55.56 min, respectively.

Figure 6 shows that when diffusion is slow, the height of the plateau is lower. The width of the plateau zone is changed on the left hand side due to a different diffusion time scale. Decreasing the default value of the diffusion coefficient by a factor of 0.1 or 0.5 increases the diffusion time scale from 0.025 s to 0.05 s and 0.25 s, respectively.

The parameter b_p describes the distribution of P between solution and capillary wall at equilibrium. Varying the buffer power b_p changes the time at which the equilibrium concentration of 0 is reached (Fig. 7). When the buffer power is larger, then there are more nutrients available for desorption and the concentration in solution

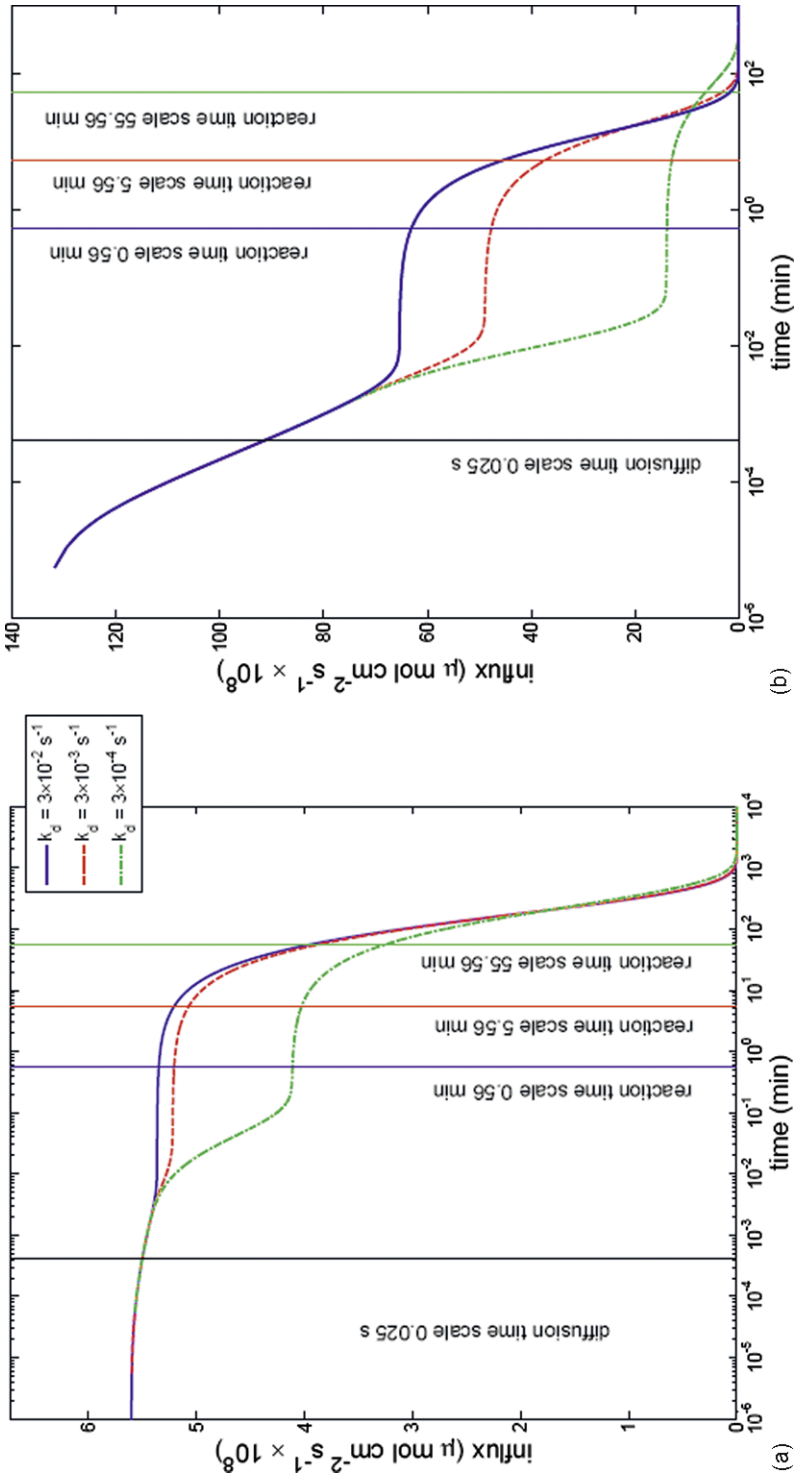

Fig. 5 Effect of varying the desorption rate constant k_d. Default parameter values: $k_d = 3 \times 10^{-2}\ \mathrm{s}^{-1}$, $C_0 = 1 \times 10^{-4}\ \mu\mathrm{mol\,cm}^{-3}$, $D_l = 1 \times 10^{-5}\ \mathrm{cm}^2\,\mathrm{s}^{-1}$, $b_p = 239$, $r_0 = 5 \times 10^{-4}$ cm, $r_1 = 25 \times 10^{-4}$ cm. (**a**) Small uptake parameter values: $K_m = 5.8 \times 10^{-3}\ \mu\mathrm{mol\,cm}^{-3}$, $F_m = 3.26 \times 10^{-6}\ \mu\mathrm{mol\,cm}^{-2}\,\mathrm{s}^{-1}$. (**b**) Large uptake parameter values: $K_m = 1.7 \times 10^{-3}\ \mu\mathrm{mol\,cm}^{-3}$, $F_m = 2.55 \times 10^{-5}\ \mu\mathrm{mol\,cm}^{-2}$

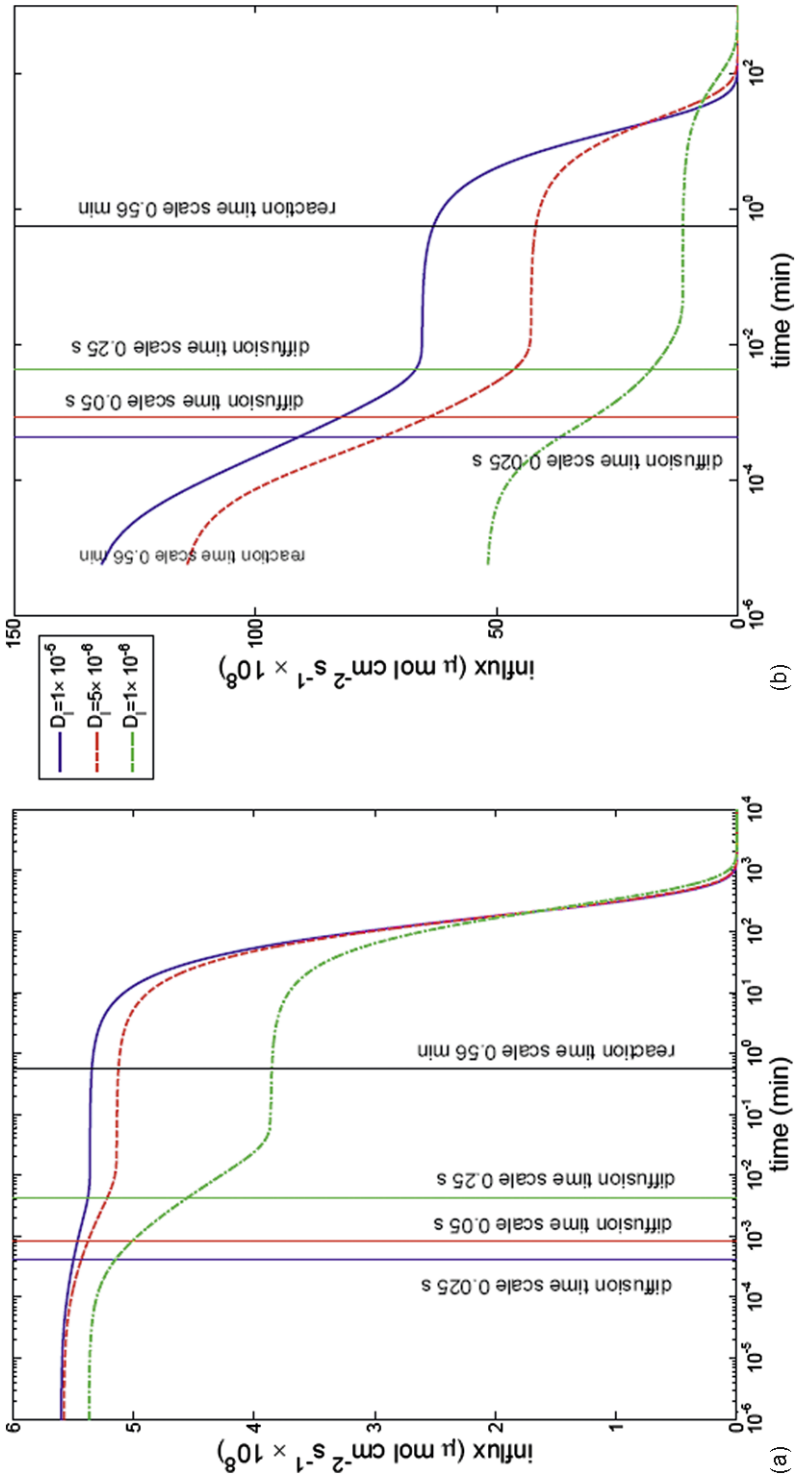

Fig. 6 Effect of varying the Diffusion coefficient D_l. Default parameter values: $k_d = 3 \times 10^{-2}\,\mathrm{s}^{-1}$, $C_0 = 1 \times 10^{-4}\,\mu\mathrm{mol\,cm}^{-3}$, $D_l = 1 \times 10^{-5}\,\mathrm{cm}^2\,\mathrm{s}^{-1}$, $b_p = 239$, $r_0 = 5 \times 10^{-4}$ cm, $r_1 = 25 \times 10^{-4}$ cm. (**a**) Small uptake parameter values: $K_m = 5.8 \times 10^{-3}\,\mu\mathrm{mol\,cm}^{-3}$, $F_m = 3.26 \times 10^{-6}\,\mu\mathrm{mol\,cm}^{-2}\,\mathrm{s}^{-1}$. (**b**) Large uptake parameter values: $K_m = 1.7 \times 10^{-3}\,\mu\mathrm{mol\,cm}^{-3}$, $F_m = 2.55 \times 10^{-5}\,\mu\mathrm{mol\,cm}^{-2}$

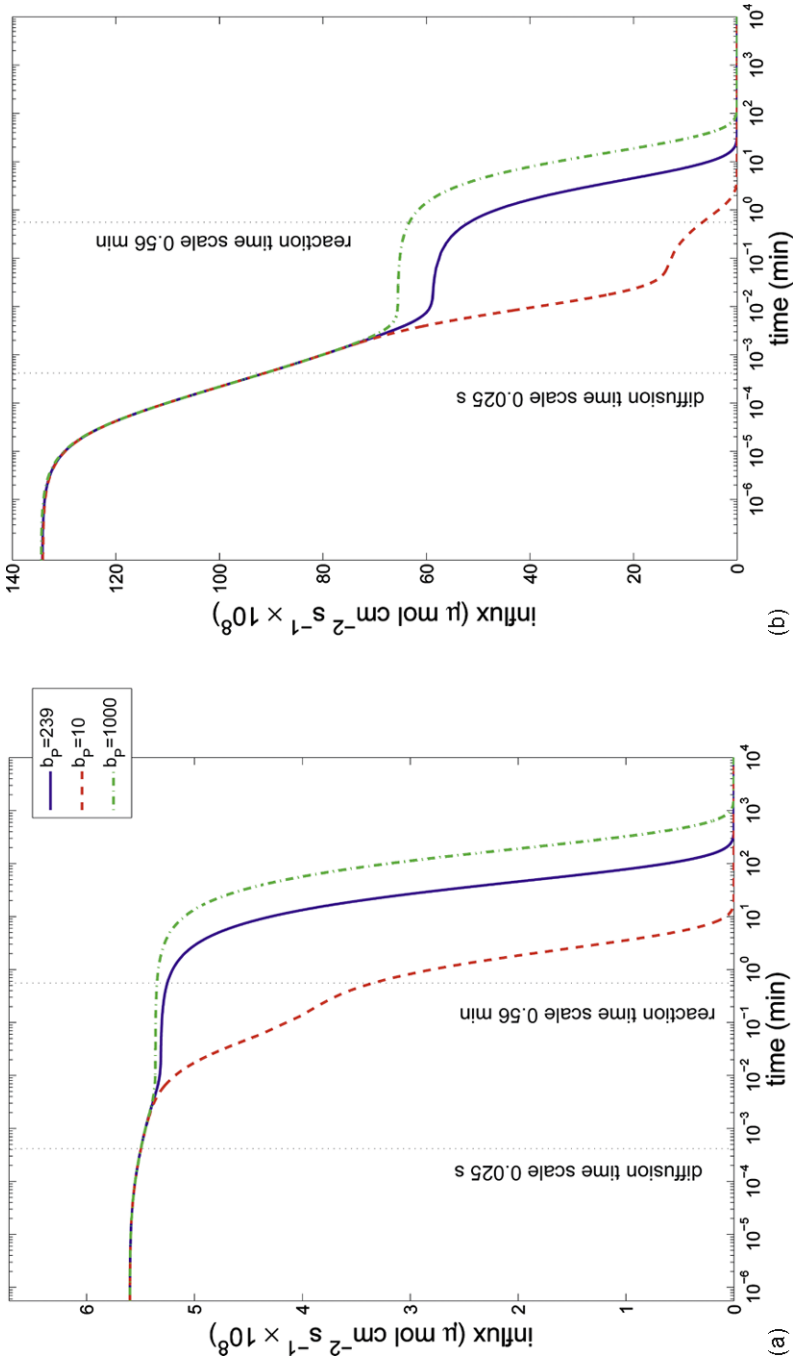

Fig. 7 Effect of varying the buffer power b_P. Default parameter values: $k_d = 3 \times 10^{-2}\,\mathrm{s}^{-1}$, $C_0 = 1 \times 10^{-4}\ \mu\mathrm{mol\,cm}^{-3}$, $D_l = 1 \times 10^{-5}\,\mathrm{cm}^2\,\mathrm{s}^{-1}$, $b_p = 239$, $r_0 = 5 \times 10^{-4}$ cm, $r_1 = 25 \times 10^{-4}$ cm. (**a**) Small uptake parameter values: $K_m = 5.8 \times 10^{-3}\ \mu\mathrm{mol\,cm}^{-3}$, $F_m = 3.26 \times 10^{-6}\ \mu\mathrm{mol\,cm}^{-2}\,\mathrm{s}^{-1}$. (**b**) Large uptake parameter values: $K_m = 1.7 \times 10^{-3}\ \mu\mathrm{mol\,cm}^{-3}$, $F_m = 2.55 \times 10^{-5}\ \mu\mathrm{mol\,cm}^{-2}$

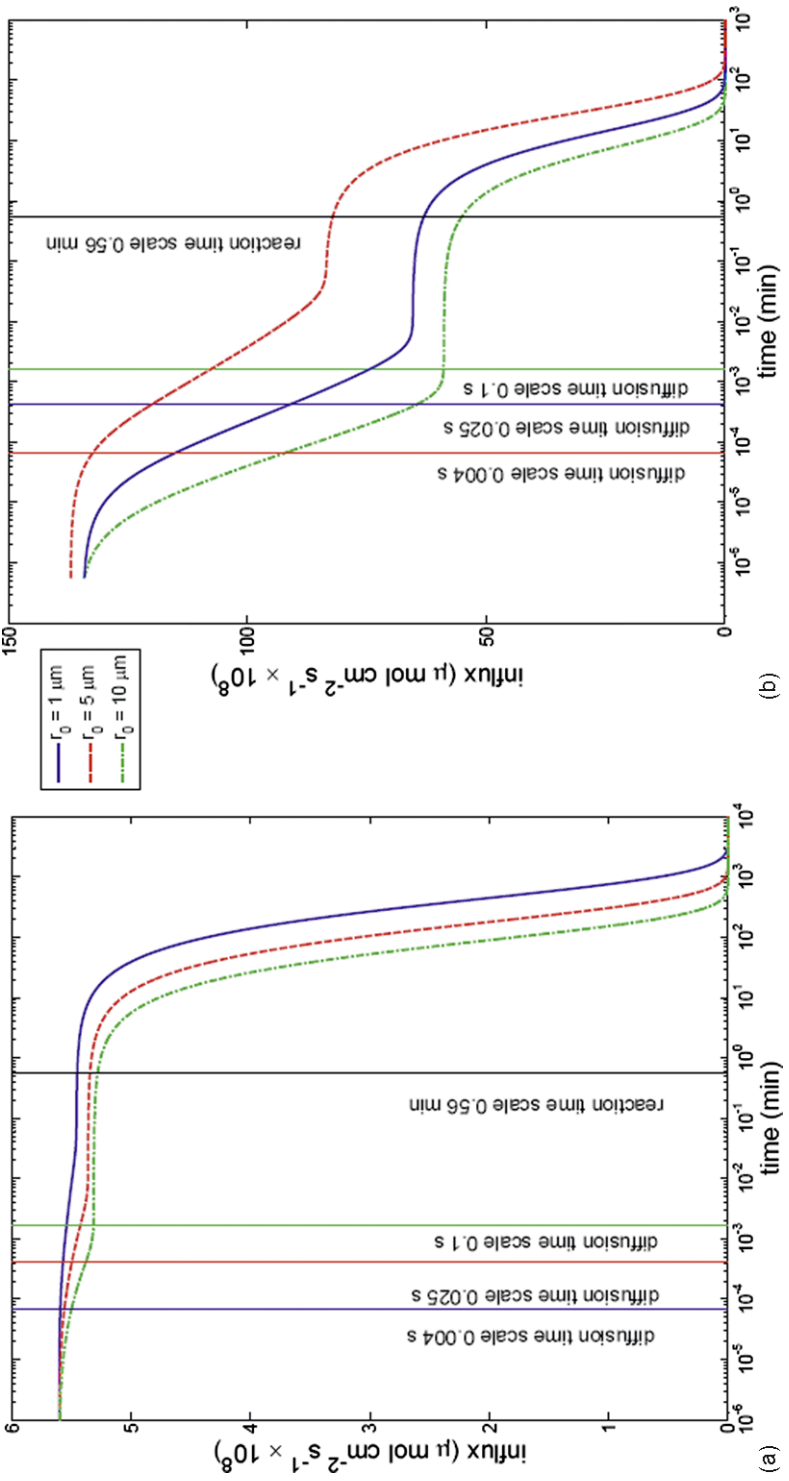

Fig. 8 Effect of varying the hyphal radius r_0. Default parameter values: $k_d = 3 \times 10^{-2}\,\mathrm{s}^{-1}$, $C_0 = 1 \times 10^{-4}$ μmol cm^{-3}, $D_l = 1 \times 10^{-5}\,\mathrm{cm}^2\,\mathrm{s}^{-1}$, $b_p = 239$, $r_0 = 5 \times 10^{-4}$ cm, $r_1 = 25 \times 10^{-4}$ cm. (**a**) Small uptake parameter values: $K_m = 5.8 \times 10^{-3}$ μmol cm^{-3}, $F_m = 3.26 \times 10^{-6}$ μmol cm$^{-2}\,\mathrm{s}^{-1}$. (**b**) Large uptake parameter values: $K_m = 1.7 \times 10^{-3}$ μmol cm^{-3}, $F_m = 2.55 \times 10^{-5}$ μmol cm^{-2}

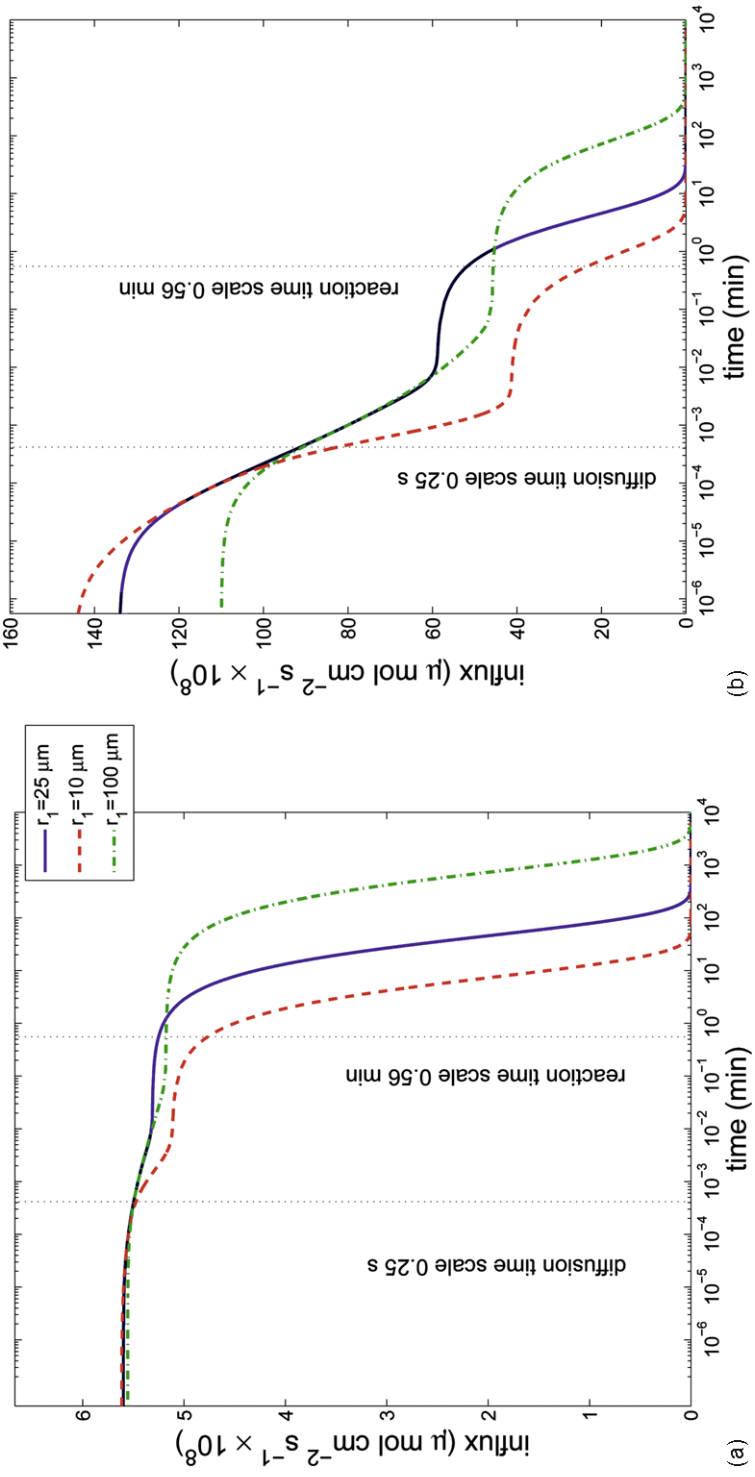

Fig. 9 Effect of varying the capillary tube radius r_1. Default parameter values: $k_d = 3 \times 10^{-2}\ \mathrm{s}^{-1}$, $C_0 = 1 \times 10^{-4}\ \mu\mathrm{mol\,cm}^{-3}$, $D_l = 1 \times 10^{-5}\ \mathrm{cm}^2\,\mathrm{s}^{-1}$, $b_p = 239$, $r_0 = 5 \times 10^{-4}$ cm, $r_1 = 25 \times 10^{-4}$ cm. (**a**) Small uptake parameter values: $K_m = 5.8 \times 10^{-3}\ \mu\mathrm{mol\,cm}^{-3}$, $F_m = 3.26 \times 10^{-6}\ \mu\mathrm{mol\,cm}^{-2}\,\mathrm{s}^{-1}$. (**b**) Large uptake parameter values: $K_m = 1.7 \times 10^{-3}\ \mu\mathrm{mol\,cm}^{-3}$, $F_m = 2.55 \times 10^{-5}\ \mu\mathrm{mol\,cm}^{-2}$

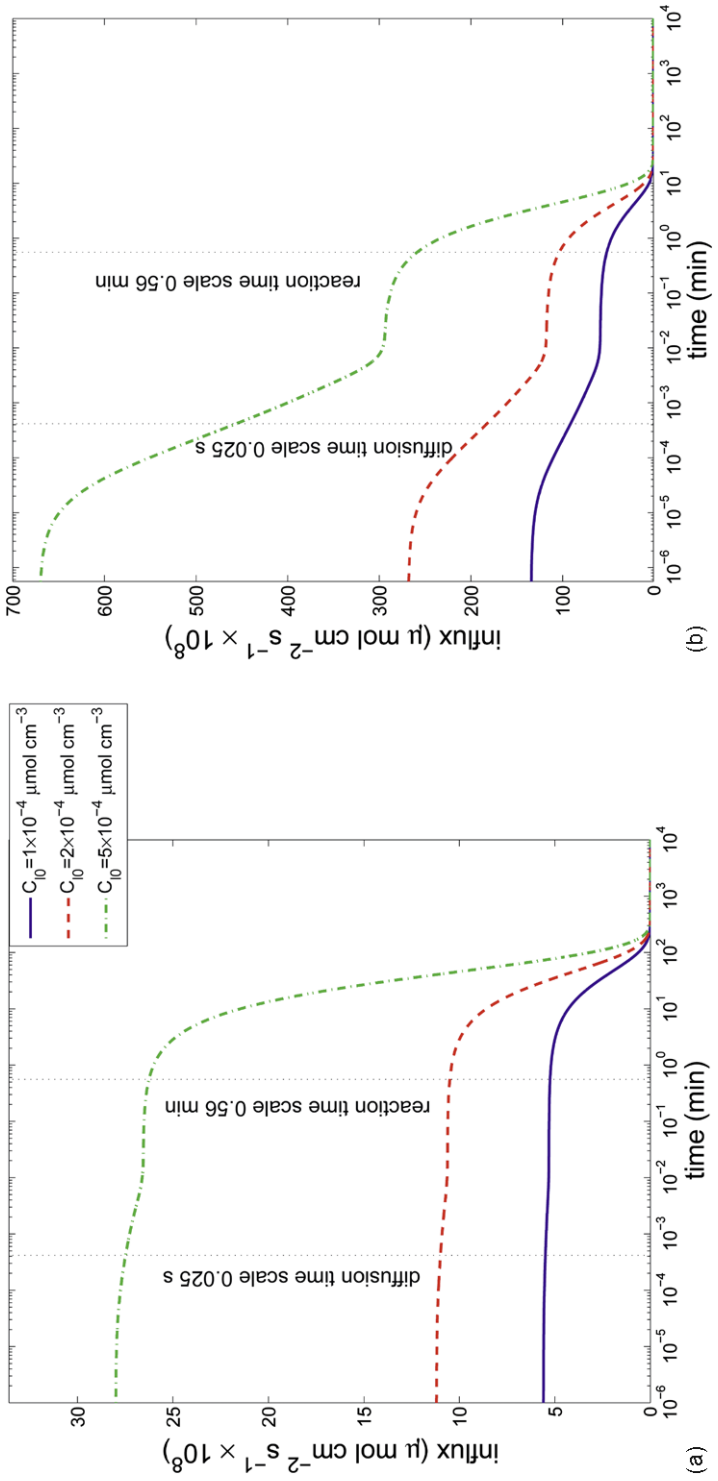

Fig. 10 Effect of varying the initial solution concentration C_{l0}. Default parameter values: $k_d = 3 \times 10^{-2}\ \mathrm{s}^{-1}$, $C_0 = 1 \times 10^{-4}\ \mu\mathrm{mol\,cm}^{-3}$, $D_l = 1 \times 10^{-5}\ \mathrm{cm}^2\,\mathrm{s}^{-1}$, $b_p = 239$, $r_0 = 5 \times 10^{-4}$ cm, $r_1 = 25 \times 10^{-4}$ cm. (**a**) Small uptake parameter values: $K_m = 5.8 \times 10^{-3}\ \mu\mathrm{mol\,cm}^{-3}$, $F_m = 3.26 \times 10^{-6}\ \mu\mathrm{mol\,cm}^{-2}\,\mathrm{s}^{-1}$. (**b**) Large uptake parameter values: $K_m = 1.7 \times 10^{-3}\ \mu\mathrm{mol\,cm}^{-3}$, $F_m = 2.55 \times 10^{-5}\ \mu\mathrm{mol\,cm}^{-2}$

can be sustained for a longer period of time. When b_P is very small, the plateau disappears because the amount of nutrients to be desorbed becomes negligibly small. Diffusion and reaction time scales are not changed by changing the buffer power b_p.

Figure 8 shows that a larger hyphal radius causes the diffusion time scale to be larger and the height of the plateau to be smaller. A smaller hyphal radius of 1 μm decreases the diffusion time scale from the default value of 0.025 s to 0.004 s; a larger hyphal radius of 10 μm increases the diffusion time scale to 0.1 s. The equilibrium concentration of 0 is reached at an earlier time when the hyphal radius is large.

Changing the radius of the capillary tube r_1 leaves the diffusion and reaction time scales the same. However, the equilibrium concentration of 0 is reached at a later time for large r_1 (Fig. 9).

Changing the initial solution concentration C_{l0} only changes the value of the initial influx and the height of the plateau, but the width of the diffusion and reaction time scale zones stay the same and the equilibrium concentration of 0 is also reached at the same time (Fig. 10). For practical applications, C_{l0} should be chosen such that P concentrations are within the detection limit of the measurement method used.

The model presented here is a tool for interpreting single hyphal scale experiments. We illustrated that the dynamics of hyphal P uptake from a capillary tube is characterised by three phases: one where the diffusion coefficient of the solution/hydrogel is important, one where the sorption properties of the capillary wall dominate, and finally one when the wall has been depleted and the final zero equilibrium is reached. Based on a default parameter set, parameter values were changed within realistic limits (see Table 1) in order to find the experimental setup most suitable with respect to time and spatial scales.

To facilitate measuring the P influx, the dynamics of P uptake should occur on a large enough time scale. Diffusion and reaction time scales can be increased by decreasing the diffusion coefficient and desorption rate constant, respectively. These abiotic factors of the experimental setup can be manipulated by using hydrogels that have a smaller diffusion coefficient than water solutions and by using different coatings on the capillary walls that effect sorption properties for P (Abdallah and Gagnon 2009; Park et al. 2009). Such hydrogels are non-toxic and have been frequently used to study the growth of plants and fungi in the laboratory (Pierard et al. 2007). Further, their chemical and physical properties can be readily manipulated to alter their diffusion properties and chemical delivery rates (Pierard et al. 2007; Moribe et al. 2008; Zheng et al. 2009). In the case of the capillary coatings, these could consist of different (oxy)hydroxides of Al and Fe, minerals which commonly occur in soil and primarily limit P availability at soil pH values <7. Depending on the parameter values used, the solution concentration inside the capillary tube can be sustained in the range of seconds to days. Comparing the effect of the parameter values of k_d and D_l on the influx into the hypha after 0.5 min, Fig. 11 shows that increasing k_d has negligible effect on the influx compared to increasing D_l. The model suggests that in order to design an experiment operating on measurable time scales, changing the diffusion coefficient, e.g., by using various hydrogels, would be most successful. This would also be suitable with the use of in vitro cultures of arbuscular mycorrhizal fungi which are typically grown on agar plates.

The choice of the spatial dimension of the capillary tube is primarily dependent on the radius of the mycorrhizal hyphae used (typically ca. 2.5 to 20 μm in width). The

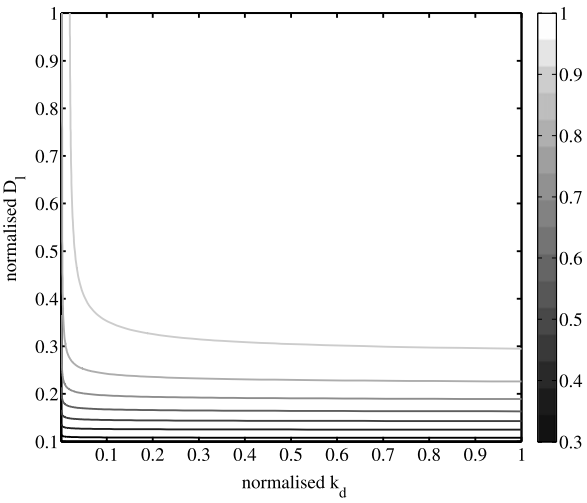

Fig. 11 Effect of varying both the parameters k_d and D_l on the calculated influx after 0.5 min

model presented here is suitable if the capillary radius is in the same order than the hyphal radius. If the capillary radius is much larger than the hyphal radius, the model changes to one with a semi-infinite domain, i.e. the capillary wall is so far away that the hypha is not affected by it. On the other hand, if the hypha were growing in a (soil) matrix with pores much smaller than the hyphal radius, the model would reduce to the situation of a continuum soil which is mostly the case for plant roots. For this situation, there exists an approximate analytical solution as detailed in Roose et al. (2001).

However, this model is based on the following assumptions that represent simplification of the real soil system:

Assuming radial symmetry with a completely fluid filled pore in which a hypha is centrally positioned might be acceptable for an artificial experimental, but is not realistic for soil situations. Pores would be filled with air as well and hyphae would not be positioned in the centre. Cameron and Buchan (2006) suggest the following soil pore classes: macro-pores 75–100 μm, meso-pores 30–75 μm, micropores 5–30 μm, ultramicropores 0.1–5 μm, crypto-pores 0.01–0.1 μm and 0.007–0.01 μm. Thus, our model is valid for soils with pores mainly in the micro- and mesopore range. In such situations, the hypha can be viewed as growing in individual soil pores instead of viewing the soil as a homogeneous matrix.

Uptake properties are likely to change along the axis of the hypha. For example, tip-localized release of *P* solubilising agents (e.g. organic acids) and uptake of *P* has been reported in some fungi (Plassard and Dell 2010). This limitation could be overcome in a 3-dimensional model where particularly the variations along the hyphal axis could be taken into account. A 3-dimensional approximation would be closer to the real soil situation. Our model can only be seen to represent a unit length of a hypha; and different characteristics might be assigned to the different units that make up the whole hypha in an upscaling process as has been done for root hairs by Leitner et al. (2010). This would also capture the limitation that we did not consider hyphal growth.

It has been shown that a hypha can modify its environment, e.g. by acidifying the region behind the tip (Jolicoeur et al. 1998), excretion of organic acids, or direct mineral weathering (Rosling et al. 2009). These processes have not been considered in this paper, but extension to this would not be impossible. Rather we consider this beyond the scope of this paper.

One could also think of an alternative experimental setup where hyphae grow into narrow gaps between glass slides. Modelling such an experimental situation would result in a 1-dimensional model or a 2-dimensional model which could take variations along hyphal axis into account. Qualitatively, results should be similar to the cylindrical case, however, if one is interested in quantitatively realistic parameter values, the cylindrical shape seems more appropriate as it mimics the soil pore situation more closely.

In conclusion, we present a mechanistic model that suggests that arbuscular mycorrhizal hyphae can rapidly deplete nutrients from soil micropores. These findings are consistent with gross spatial scale experimental measurements made in soil. This analysis will help to design relevant single hyphal scale experiments.

Acknowledgements We acknowledge the FWF Austrian Science Fund (Projects P15749, T341-N13) for financial support. Tiina Roose is a Royal Society University Research Fellow. Davey Jones was supported by the UK Biotechnology and Biological Sciences Research Council.

References

Abdallah, E. A. M., & Gagnon, G. A. (2009). Arsenic removal from groundwater through iron oxyhydroxide coated waste products. *Can. J. Civ. Eng.*, *36*, 881–888.

Abu Ali, R., Murphy, R. J. & Dickinson, D. J. (1999). Investigation of the extracellular mucilaginous materials produced by some wood decay fungi. *Mycol. Res.*, *103*, 1453–1461.

Allen, M. F. (2007). Mycorrhizal fungi: Highways for water and nutrients in arid soils. *Vadose Zone J.*, *6*, 291–297.

Barber, S. A. (1995). *Soil nutrient bioavailability: a mechanistic approach*. New York: Wiley.

Boyle, J. R., & Voigt, G. K. (1973). Biological weathering of silicate minerals. *Plant Soil*, *38*, 191–201.

Cameron, K. C., & Buchan, G. D. (2006). Porosity and pore size distribution. In R. Lal (Ed.), *Encyclopedia of soil science* (pp. 1350–1353). Boca Raton: CRC Press.

Chen, J. S., Mansell, R. S., Nkedi-Kizza, P., & Burgoa, B. A. (1996). Phosphorus transport during transient, unsaturated water flow in an acid sandy soil. *Soil Sci. Soc. Am. J.*, *60*, 42–48.

Crank, J. (1975). *The mathematics of diffusion*. Oxford: Clarendon Press.

da Silveira, A. P. D., & Cardoso, E. J. B. N. (2004). Arbuscular mycorrhiza and kinetic parameters of phosphorus absorption by bean plants. *Sci. Agric.*, *61*, 203–209.

Darrah, P. R., Jones, D. L., Kirk, G. J. D., & Roose, T. (2006). Modelling the rhizosphere: a review of methods for 'upscaling' to the whole-plant scale. *Eur. J. Soil Sci.*, *57*, 13–25.

Deressa, T. G., & Schenk, M. K. (2008). Contribution of roots and hyphae to phosphorus uptake of mycorrhizal onion (*Allium cepa* L.)—a mechanistic modeling approach. *J. Plant Nutr. Soil Sci.*, *171*, 810–820.

Ezawa, T., Smith, S. E., & Smith, F. A. (2002). P metabolism and transport in AM fungi. *Plant Soil*, *244*, 221–230.

Facelli, E., Smith, S. E., Facelli, J. M., Christophersen, H. M., & Smith, F.A. (2010). Underground friends or enemies: model plants help to unravel direct and indirect effects of arbuscular mycorrhizal fungi on plant competition. *New Phytol.*, *185*, 1050–1061.

Fowler, A. C. (1997). *Mathematical models in the applied sciences*. Cambridge: Cambridge University Press.

Hinsinger, P., Gobran, G. R., Gregory, P. J., & Wenzel, W. W. (2005). Rhizosphere geometry and heterogeneity arising from root-mediated physical and chemical processes. *New Phytol.*, *168*, 293–303.

Jakobsen, I., Abbott, L. K., & Robson, A. D. (1992). External hyphae of vesicular-arbuscular mycorrhizal fungi associated with Trifolium subterraneum L. 1. Spread of hyphae and phosphorus inflow into roots. *New Phytol.*, *120*, 371–380.

Jolicoeur, M., Germette, S., Gaudette, M., Perrier, M., & Bécard, G. (1998). Intracellular pH in Arbuscular Mycorrhizal Fungi: a symbiotic physiological marker. *Plant Physiol.*, *116*, 1279–1288.

Jones, D. L., & Hinsinger, P. (2008). The rhizosphere: complex by design. *Plant Soil*, *312*, 1–6.

Jones, D. L., Hodge, A., & Kuzyakov, Y. (2004). Plant and mycorrhizal regulation of rhizodeposition. *New Phytol.*, *163*, 459–480.

Jongmans, A. G., Van Breemen, N., Lundström, U., Van Hees, P. A. W., Finlay, R. D., Srinivasan, M., Unestam, T., Giesler, R., Melkerud, P. A., & Olsson, M. (1997). Rock-eating fungi [4]. *Nature*, *389*, 682–683.

Kirk, G. J. D., Santos, E. E., & Santos, M. B. (1999). Phosphate solubilization by organic anion excretion from rice growing in aerobic soil: Rates of excretion and decomposition, effects on rhizosphere pH and effects on phosphate solubility and uptake. *New Phytol.*, *142*, 185–200.

Koorevaar, P., Menelik, G., & Dirksen, C. (1983). *Elements of soil physics*. Amsterdam: Elsevier.

Krcmar, P., Novotny, C., Marais, M. F., & Joseleau, J. P. (1999). Structure of extracellular polysaccharide produced by lignin-degrading fungus Phlebia radiata in liquid culture. *Int. J. Biol. Macromol.*, *24*, 61–64.

Leigh, J., Hodge, A., & Fitter, A. H. (2009). Arbuscular mycorrhizal fungi can transfer substantial amounts of nitrogen to their host plant from organic material. *New Phytol.*, *181*, 199–207.

Leitner, D., Klepsch, S., Ptashnyk, M., Marchant, A., Kirk, G. J. D., Schnepf, A., & Roose, T. (2010). A dynamic model of nutrient uptake by root hairs. *New Phytol.*, *185*, 792–802.

Lide, D. R. (2000). *Handbook of chemistry and physics* (83th ed.) Boca Raton: CRC Press.

Mackay, A. D., & Barber, S. A. (1985). Soil-moisture effect on potassium uptake by corn. *Agron. J.*, *77*, 524–527.

McKeague, J. A., Chesire, M. V., Andreux, F., & Berthelin, J. (1986). Organo mineral complexes in relation to pedogenesis. In P. M. Huang, M. Schnitzer (Eds.), *Interactions of soil minerals with natural organics and microbes* (pp. 549–592). Madison: SSSA.

Moribe, K., Nomizu, N., Izukura, S., Yamamoto, K., Tozuka, Y., Sakurai, M., Ishida, A., Nishida, H., & Miyazaki, M. (2008). Physicochemical morphological and therapeutic evaluation of agarose hydrogel particles as a reservoir for basic fibroblast growth factor. *Pharm. Dev. Technol.*, *13*, 541–547.

Ockendon, H., & Ockendon, J. R. (1995). *Cambridge texts in applied mathematics*. *Viscous flow*. Cambridge: Cambridge University Press.

Park, C. D., Walker, J., Tannenbaum, R., Stiegman, A. E., Frydrych, J., & Machala, L. (2009). Sol-gel-derived iron oxide thin films on silicon: surface properties and interfacial chemistry. *ACS Appl. Mater. Interfaces*, *1*, 1843–1846.

Pierard, G. E., Pierard-Franchimont, C., & Quatresooz, P. (2007). Fungal thigmotropism in onychomycosis and in a clear hydrogel pad model. *Dermatoloty*, *215*, 107–113.

Plassard, C., & Dell, B. (2010). Phosphorus nutrition of mycorrhizal trees. *Tree Physiol.*, *30*, 1129–1139.

Roose, T., & Schnepf, A. (2008). Mathematical models of plant-soil interaction. *Philos. Trans. R. Soc., Math. Phys. Eng. Sci.*, *366*, 4597–4611.

Roose, T., Fowler, A., & Darrah, P. (2001). A mathematical model of plant nutrient uptake. *J. Math. Biol.*, *42*, 347–360.

Rosling, A., Roose, T., Herrmann, A. M., Davidson, F. A., Finlay, R. D., & Gadd, G. M. (2009). Approaches to modelling mineral weathering by fungi. *Fungal Biol. Rev.*, *23*(4), 138–144.

Saleque, M. A., & Kirk, G. J. (1995). Root-induced solubilization of phosphate in the rhizosphere of lowland rice. *New Phytol.*, *129*, 325–336.

Schnepf, A., & Roose, T. (2006). Modelling the contribution of arbuscular mycorrhizal fungi to plant phosphate uptake. *New Phytol.*, *171*, 669–682.

Schnepf, A., Roose, T., & Schweiger, P. (2008). Impact of growth and uptake patterns of arbuscular mycorrhizal fungi on plant phosphorus uptake—a modelling study. *Plant Soil*, *312*, 85–99.

Schweiger, P., & Jakobsen, I. (1999). The role of mycorrhizas in plant P nutrition: Fungal uptake kinetics and genotype variation. In G. Gissel-Nielsen, A. Jensen (Eds.), *Plant nutrition—molecular biology and genetics* (pp. 277–289). Dordrecht: Kluwer Academic.

Schweiger, P., & Jakobsen, I. (2000). Laboratory and field methods for measurement of hyphal uptake of nutrients in soil. *Plant Soil*, *226*, 237–244.

Sharma, A. K., Srivastava, P. C., & Johri, B. N. (1999). Multiphasic zinc uptake system in mycorrhizal and nonmycorrhizal roots of French bean (Phaseolus vulgaris L.). *Curr. Sci.*, *76*, 228–230.

Smith, S. E., Smith, F. A., & Jakobsen, I. (2003). Mycorrhizal fungi can dominate phosphate supply to plants irrespective of growth responses. *Plant Physiol.*, *130*, 16–20.

Staddon, P. L., Ramsey, C. B., Ostle, N., Ineson, P., & Fitter, A. H. (2003). Rapid turnover of hyphae of mycorrhizal fungi determined by AMS microanalysis of 14C. *Science*, *300*, 1138–1140.

Tinker, P. B., & Nye, P. H. (2000). *Solute movement in the rhizosphere*. London: Oxford University Press.

Van Breemen, N., Finlay, R., Lundström, U., Jongmans, A. G., Giesler, R., & Olsson, M. (2000). Mycorrhizal weathering: a true case of mineral plant nutrition? *Biogeochemistry*, *49*, 53–67.

Zheng, T., Liang, Y. H., Ye, S. H., & He, Z. Y. (2009). Superabsorbent hydrogels as carriers for the controlled-release of urea: experiments and a mathematical model describing the release rate. *Biosyst. Eng.*, *102*, 44–50.